

Simulating Electric-Vehicle Battery Degradation with Physics Based Battery Model^{*}

Lucas S. Teixeira^{*} Sidelmo M. da Silva^{**}

^{*} Programa de Pós-Graduação de Engenharia Elétrica, Universidade Federal de Minas Gerais, MG (e-mail: lucas.sarvtex@gmail.com).

^{**} Escola de Engenharia, Universidade Federal de Minas Gerais, MG (e-mail: sidelmosilva@gmail.com)

Abstract: Physics-based mathematical representations of batteries are the most complete and complex battery models in the literature. These models are exemplified by PyBaMM; a well documented, easy to use, open-source python library which can be used to simulate physics-based battery models of various levels of complexity and detail. This work describes the process, the workflow and the viability of combining an Electric Vehicle powertrain model, constructed in Simulink, with a PyBaMM model in order to observe an accelerated battery degradation cycle using a physics-based model.

Keywords: Li-Ion Batteries, Battery Degradation, Electric-Vehicles, PyBaMM, Simulink.

1. INTRODUCTION

The electrification of the transport sector is an important step in the energy transition towards cleaner sources of energy. Recent improvements to battery technologies have made electric vehicles cheaper, more reliable, and more viable alternatives to traditional combustion vehicles.

However, the current generation of battery technology is still flawed. Energy and power densities are still relatively small, leading to limited driving ranges. Additionally, these batteries have limited lifespan due to capacity and power degradation; once a battery reaches 80% of its original capacity, it is advised that it be replaced. After this first end-of-life, the battery can still be reused in less power and capacity intensive stationary applications. This phase is known as the “Second Life” for the battery (Martinez-Laserna et al., 2018).

This work contributes to a larger project which aims to study Second Life Batteries. The focus during this initial stage is to study the patterns of long-term Li-ion battery degradation with a specific focus on simulation.

Modelling battery degradation is important for both first and second life applications. Typically in electrical engineering this is done using an empirical model, a set of mathematical equations that relate stress-factors such as average temperature, Depth-of-Discharge, and average State-of-Charge with capacity loss and impedance increase (Hu et al., 2019). Empirical models are agnostic about the internal mechanisms of battery aging and rely instead on macroscopic heuristic relations; this makes these model simple but less reliable in extreme circumstances.

^{*} This work was supported in part by the Brazilian federal government agencies Coordenação de Aperfeiçoamento de Pessoal de Nível Superior (CAPES), and Conselho Nacional de Desenvolvimento Científico e Tecnológico (CNPq). The authors also would like to thank the Graduate Program in Electrical Engineering of the Federal University of Minas Gerais

Physics-based battery models explicitly represent the internal physical and chemical state of the battery cell, they are more complex but also more accurate for a larger share of battery use-cases. Hu et al. (2022) finds it to be the best method to model long-term degradation in general and second-life degradation in particular.

This work combines a physics-based model (created using the Python library ‘PyBaMM’) and an Electric Vehicle model (built in Simulink). This ensures that the most advanced kind of battery model is available for use in MATLAB, a common simulation tool for engineers and academia.

2. MODELLING AN ELECTRIC VEHICLE

To model battery degradation in the context of an Electric Vehicle (EV), the vehicle itself must first be modelled. To do so, it is useful to break the problem down into its component parts, and model each of these individually.

Given that this work focuses on vehicular motion and power consumption, the most relevant system to model is the *powertrain*. This system is the single most important one in any vehicle; it is tasked with converting energy in the storage system and delivering it to the propulsion system (Alcantara, 2022; Ehsani et al., 2018; Oliveira et al., 2023). This system can be further disassembled into a chain of components. In an BEV, these components are: **battery pack**, **power inverter**, **electric motor**, and the **propulsion system**. During acceleration, as power flows from the former to the latter, each of these components provides current, power, or torque from the one immediately proceeds it (Zhou, 2007); this hierarchy is shown in Figure 1, adapted from Miri et al. (2021).

This work considers a simplified mathematical EV model. Section 2.1 discusses the propulsion system and the movement dynamics. Section 2.2 discusses the Electric Motor

and Inverter. Lastly, Section 2.3 deals with the topic of regenerative braking.

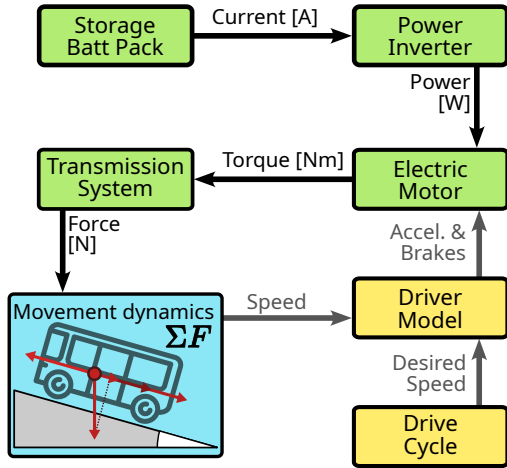


Figure 1. Diagram of simplified vehicle model. Green blocks represent Powertrain components, yellow represents control blocks. Adapted from Miri et al. (2021); Zhou (2007).

2.1 Propulsion System and Movement Dynamics

The propulsion system is closely tied to the movement of the vehicle, whose dynamics can be modelled with a simple model. Equation (1) describes vehicular acceleration; where v is vehicle speed (in m/s), M represent the overall mass of the vehicle, and k_m represents the rotational inertial factor (a property of the transmission system, typically around 1.3) (Ehsani et al., 2018). Equation (2) shows the sum of forces which acts upon the vehicle (ΣF).

$$\partial v / \partial t = \Sigma F / (k_m \cdot M), \quad (1)$$

$$\Sigma F = F_{pr} - F_G - F_{drag} - F_{rr}. \quad (2)$$

Here, the propelling force (F_{pr}) is the one controllable component, it originates from the transmission system through the motor or brakes. The gravitational force (F_G) may contribute to acceleration or deceleration, depending on road inclination; its behaviour is described by (3), where g is the gravitational acceleration and θ is the angle of the road. Drag force and rolling resistance (F_{drag} and F_{rr} , respectively) are resistance forces, always acting against the direction of velocity. Drag is caused by air resistance; it is mathematically described by (4) where ρ is air density, A is the frontal area of the vehicle and C_d is the air drag coefficient. Rolling resistance is caused by tire deformation and friction between tire and road; it is described by (5) where C_r is the rolling resistance coefficient (Oliveira et al., 2023; Alcantara, 2022).

$$F_G = k_m M g \cdot \sin(\theta) \quad (3)$$

$$F_{drag} = \frac{1}{2} \cdot \rho A C_d \cdot v^2 \quad (4)$$

$$F_{rr} = M g \cdot C_r \cdot \cos(\theta) \quad (5)$$

2.2 Motor and Inverter

The motor and the inverter are intermediate components between the battery storage system and the propulsion system. During acceleration, these elements “demand”

from the storage unit a given amount of power (P_{batt}) and “deliver” to the vehicle the necessary propelling force (F_{pr}).

At any given rotational velocity, the motor is limited in the maximum amount of torque that it is able to provide. These constraints are described by the motor Torque-curve, shown in Figure 2. For rotational speeds below a certain v_{base} , the motor is limited by a maximum torque value (T_m^{max}); for speeds above v_{base} , the motor is limited by the motor power capacity (P_m^{max}).

The relationship between motor torque and propelling force is given by (6); and the relationship between motor rotational speed and vehicle longitudinal velocity is given by (7). Here, η_t is the transmission efficiency, r_w is the wheel radius, and G represents the transmission gear ratio (Oliveira et al., 2023). Electric Vehicles are characterized by the presence of a single gear ratio – which means that there is only a single, constant value for G . This is in contrast with combustion engine powered vehicles, which require many gear ratios to operate effectively at different speed ranges. The simplified transmission system is one of the inherit advantages of electric vehicles (Ehsani et al., 2018).

$$F_{pr} = (G/r_w) \cdot \eta_t \times T_m \quad (6)$$

$$v = (r_w/G) \times \omega_m \quad (7)$$

During acceleration, the output propulsion power (P_{pr}) delivered by the electric motor – given by (8) – is smaller than delivered from the energy storage system to the inverter (P_{batt}). This is due to losses within the motor-inverter system. In this scenario, the power extracted from the battery pack is described by (9), where η_{mi} is the electrical efficiency of the motor-inverter system, a value between 0 and 1. This efficiency value can be defined as a constant, though it is typically described as a function of torque and rotor speed; Figure 2 shows a motor-inverter efficiency map along side a motor torque-curve (Miri et al., 2021).

$$P_{pr} = F_{pr} \cdot v \quad (8)$$

$$P_{batt} = P_{pr} / \eta_{mi}(T, \omega) \quad (9)$$

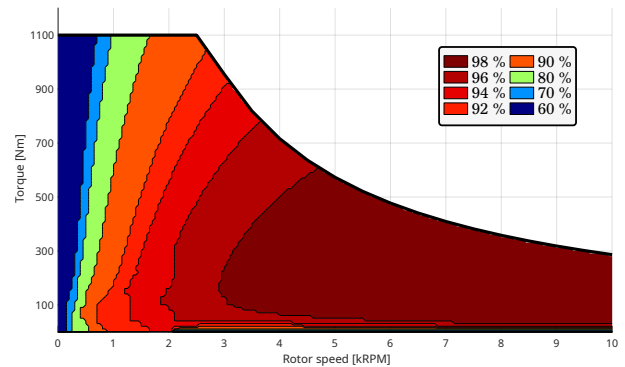


Figure 2. Torque-curve graph with efficiency map. Black line shows max available torque at any given speed, colors indicate Motor/Inverter system electric efficiency. Adapted from Mahmoudi et al. (2015).

2.3 Regenerative braking

Commercial electric vehicles include two modes of braking: friction and regenerative. Friction brakes decelerate the

vehicle by dissipating the kinetic energy into sound and heat. This is the standard kind of brake present in most ICE vehicles. Electric vehicles, by contrast, are able to recharge during deceleration. This is due to the capacity of any electric motor to function as a generator. This ability to charge the battery by braking during driving guarantees extended driving range for EVs (Alcantara, 2022).

Regenerative braking is, however, limited. For one, it is inefficient at low speeds, unsafe when deceleration is too high, and unnecessary if the battery is nearly full; in those circumstances, the friction brakes are used instead. Additionally, it is constrained by a maximum power limit (P_{reg}^{max}) which is typically smaller than the motor max power output (Miri et al., 2021). All of this considered, the power delivered to the battery from regenerative braking is given by (10). Here, α is a value which varies between 0 and 1 depending on velocity, deceleration rate and battery SoC; as per Miri et al. (2021). Note also that, as per (8), P_{pr} is negative when braking.

$$P_{batt} = \eta_{mi} \times \begin{cases} \alpha \cdot P_{pr}, & \text{if } |\alpha \cdot P_{pr}| \leq |P_{reg}^{max}| \\ P_{reg}^{max}, & \text{otherwise} \end{cases} \quad (10)$$

2.4 Drive cycle and Driver

To represent driver behaviour, this work uses a PI controller model, shown in Figure 3, adapted from Miri et al. (2021). A custom drive-cycle (longitudinal speed over time) made by Alcantara (2022) is used as the reference speed input; this value is compared to the measured output vehicle velocity. The output of the PI controller is a value between 1 and -1 which is interpreted as pedal commands for the accelerator (if positive) and brake (if negative).

These pedal commands control the output propulsion and braking force as described by (11) and (12). In equation (11), a_{acc} represents the acceleration command and $F_{mi}^{max}(v)$ is the maximum force available for a given velocity v , as per the torque-curve and equations (6) and (7). In equation (12), a_{brk} is the braking pedal command and F_{br}^{max} is the maximum brake force is given by (13), where k_{ad} is the adhesion coefficient (around 0.8 for dry asphalt conditions) (Miri et al., 2021).

The parameters for the PI controller were chosen following trial-and-error simulations in order to minimize the RMSE error between reference and measured speed (Oliveira et al., 2023).

$$F_{pr} = a_{acc} \cdot F_{mi}^{max}(v) \quad (11)$$

$$F_{br} = a_{brk} \cdot F_{br}^{max} \quad (12)$$

$$F_{br}^{max} = k_{ad} \cdot Mg \quad (13)$$

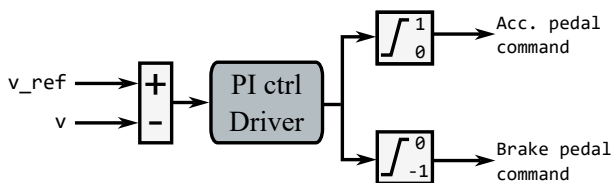


Figure 3. PI controller driver model.

3. MODELLING LI-ION BATTERIES

The storage system is the single most important component in an Electric Vehicle. Not only do battery packs represent a plurality of the total cost, it is only due to recent cost reductions and improvements in battery technologies (particularly within lithium based chemistries) that EVs are at all viable. Despite that, batteries themselves are complex, non-linear, electrochemical systems which are inherently hard to model.

Within electrical engineering, Equivalent Circuit Models (ECMs) is the technique most commonly used to represent batteries. These models use a variable voltage source and passive elements (resistors and capacitors) to represent the dynamic response and ohmic losses (Hu et al., 2012). To account for capacity and power loss which come with aging, ECMs typically rely on an external aging model, of which there are three main types: empirical, mechanistic, and data-driven (Hu et al., 2020). Empirical models, the simplest and most common ones, are based on establishing heuristic correlations (expressed in simpler mathematical equations) between capacity fade and impedance increase, and identified stress factors such as temperature, average SoC, depth-of-discharge, and others (Ganesh and D’Arpino, 2023; Hu et al., 2019). This approach is easy to implement and is very computationally simple; however, it has relatively low-accuracy and is typically only “tuned” for a limited set of operating conditions (often these models are calibrated in ideal laboratory conditions). These limitations mean this approach is not ideal for simulating long-term degradation trends, which is the case in Second Life applications (Hu et al., 2022).

For these more advanced applications, a mechanistic aging model is more appropriate. These models are extensions of physics-based battery cell models, an alternative to ECMs which do model the internal electrochemical phenomena mathematically. Consequentially, they are more accurate and robust, though they also require significantly more detailed parametrization and are much more complex computationally. This work will make use of these mechanistic degradation models. Section 3.1 explains the basics of physics-based battery models; section 3.2 introduces to the main kinds of degradation mechanism within a battery cell and how each is modelled mathematically.

3.1 Physics-based Battery Cell Models

Physics-based battery models arise out of electrochemistry (Newman and Balsara, 2021). The goal is to represent the internal chemical state of a single battery cell by modelling the reactions and movement of particles which take place within the system. Most of the existing electrochemical models are based on the Doyle-Fuller-Newman (DFN) model first described in Doyle et al. (1993) and Fuller et al. (1994).

Inside each battery cell, there are three regions: the negative electrode, separator, and positive electrode. The electrode regions each have their own “active-material” (alternatively called the “solid-phase”) which holds onto lithium atoms. The transfer of these lithium atoms between the two electrodes occurs during charge and discharge. This is possible due to the liquid electrolyte medium which

permeates the battery and allows for the movement of ions between the two electrode regions (Newman and Balsara, 2021; Marquis, 2020).

The DFN model represents this system as a continuum model. Most variables change continuously along a one-dimensional x -axis that starts in the negative electrode current collector ($x=0$) and ends in the positive electrode current collector ($x=L$). The one exception is lithium concentration in the active material, which may vary between the surface and the core of the solid-phase within a given x value. In DFN, this variable is modelled as varying along side the microscopic radius of a spherical solid-phase particle (r -axis) as well as cell length (x -axis). Because of this, this model is also known as “Pseudo two-dimensional” (P2D). Figure 4 shows an illustrative schematic of the DFN model, adapted from Lee and Onori (2021).

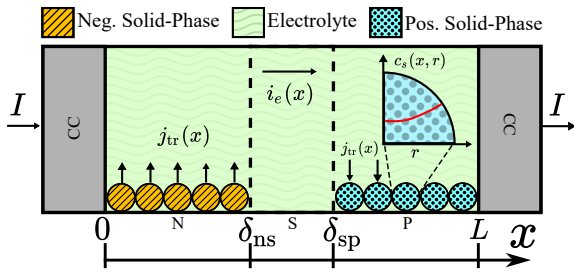


Figure 4. DFN model diagram, adapted from Lee and Onori (2021).

The DFN model can be broken down into three main phenomena. Charge conservation governs how the voltage potential in solid-phase and in the electrolyte (ϕ_s and ϕ_e) changes in response to internal currents and movement of ions. Lithium diffusion describes how the lithium concentration varies within the electrolyte and within the solid-phases (c_e and c_s) – note that lithium concentration on the surface of the electrode (c_{ss}) is the most important variable for setting the solid-phase voltage potential which itself is closely associated with open circuit cell voltage. Transfer current describes the rate of the redox chemical equations which causes the transfer of lithium ions from the solid-phase into the electrolyte and vice-versa (j_{tr}). When taken together, these processes are described by dozens of interacting Partial Differential Equations with non-linear elements. Mathematically describing this model is outside of the scope of this work. Richardson et al. (2022) is a good introduction to the mathematical side of this theory for those without a background in electrochemistry; see also Thomas et al. (2002); Prada et al. (2012) and Hariharan et al. (2018).

The DFN model is accurate for a wide range of scenarios, but it is also very computationally complex. Depending on the application, it may be possible to use a simplified version of the DFN. For example, Subramanian et al. (2005) simplifies the diffusion equations and eliminates the r -axis by representing the solid-phase lithium concentration through polynomial equations. Alternatively, the Single Particle Model (SPM) assumes that both the positive and negative electrode regions are uniform such that each can each be represented with a single particle (Guo et al., 2010; Prada et al., 2012). These simplified models can be

significantly faster than the original, though they often fail to replicate cell behaviour at high C-rate values.

3.2 Mechanistic Degradation Models

Battery degradation is the result of unintended side-reactions and mechanical stresses which occur within the cell. The four types of degradation are Loss of Lithium Inventory (LLI), Loss of Active Material (LAM), Loss of Electrolyte (LE) and Resistance Increase (RI); the effects of aging are, primarily, capacity and power fade (Han et al., 2019; Hu et al., 2020). Though the original DFN does not account for the possibility of degradation, additional equations can be added to the model to represent these processes.

The single most significant battery degradation stress factor is cell temperature (Waldmann et al., 2014), an important component of which is caused by heat generated within the battery itself. The simplest thermal model which represents internal heat generation within a battery cell is the so called ‘lumped’ model; named such because it assumes a uniform cell temperature (T_{cell}) constant throughout the entire battery. Equation (14) shows a basic implementation of this thermal model, where T_{amb} is the ambient temperature, U is open-circuit potential (dependent on surface electrode concentration, c_{ss}), C_p is cell heat capacity, h is the cell convective coefficient, and A_c and M_c are the cell’s surface area and mass, adapted from Prada et al. (2012).

$$M_c C_p \cdot \frac{dT}{dt} = ((U - V) \cdot I - h A_{cell} \cdot (T_{cell} - T_{amb})) \quad (14)$$

As for the degradation mechanisms themselves, there are many chemical side-reactions which contribute to aging, some more significant than others. To properly model a battery, one should ideally model multiple degradation mechanisms in order to better replicate the emergent behaviour from the interaction between these multiple mechanisms (Reniers et al., 2019; Edge et al., 2021). For example, Yang et al. (2017) is able to replicate the accelerated loss of capacity which occurs at the very end of a battery life-cycle (known as ‘aging knee-point’) by combining three degradation mechanisms:

- **SEI Growth:** Solid Electrolyte Interface (SEI) is a layer of organic material between the negative electrode and the electrolyte. This is the most significant source of degradation for the initial stages of the battery cell life. It is governed by complex mechanism, as such, there are competing approaches for modelling it mathematically (Reniers et al., 2019; Single et al., 2018).
- **Li plating:** Lithium ions deposited as metallic particles on the electrode-electrolyte border. Accelerates significantly near the End-of-Life, triggering the aging kneepoint. Can also be caused by fast charging and low temperatures (Yang et al., 2017; Edge et al., 2021).
- **Pore-clogging:** As the SEI and Li-plating films grow, they take up space previously occupied by the electrolyte. This leads to a decrease of electrolyte porosity. Low porosity causes the acceleration of Li-plating (Yang et al., 2017; Reniers et al., 2019).

These three degradation models reinforce each other. In doing so, they recreate real battery cell behaviour. Yang et al. (2017) was the first to replicate the aging knee-point using these mechanistic models. Since then, others have replicated this finding using modified and/or additional SEI and plating models, see Atalay et al. (2020); Müller et al. (2019) and O’Kane et al. (2022). The goal for this work is to replicate the aging knee-point curve using these basic degradation model components.

4. SIMULATION DEMONSTRATION

This simulation attempts to combine a drive-cycle controlled electric vehicle model with a physics-based battery model in order to simulate degradation using the more advanced mechanistic SEI and plating models. The goal is to replicate the plating triggered aging-knee-point demonstrated in Yang et al. (2017); Atalay et al. (2020) and others.

The electric vehicle powertrain is modelled using MATLAB/Simulink, based off the equations described in Section 2. The drive-cycle data used in this test is of a bus route within the UFMG Pampulha Campus, measured by Alcantara (2022); the drive-cycle time-step is equal to $dt = 1s$. Once the drive-cycle ends, the vehicle parks for 5 minutes and the process starts over again; this is repeated for 10 hours or until battery SoC reaches 10%. Table 1 lists the parameters being used in the Simulink model, including information for the electric bus (BYD, 2022) – including the PI values for the driver model – and the battery thermal model (Prada et al., 2012; Taylor, 2023).

To model and simulate the battery, PyBaMM (Python Battery Mathematical Modelling) – an open-source battery simulation library available for Python – was chosen (Sulzer et al., 2021). It codifies and solves various physics-based battery models using systems of differential equations. As a modelling tool, it is very flexible; it includes battery models of different levels of complexity, many options for degradation mechanisms, and some pre-installed battery parameter sets from the literature. It also has very thorough and didactic documentation available online (Marquis, 2020; Sulzer et al., 2021).

Though not a built-in functionality, communication between PyBaMM and Simulink is possible as first demonstrated in Tranter (2021). Note that adjustment are required due to this being an older version of PyBaMM.

A challenge for physics-based battery models is the large number of parameters needed to describe the system. For this work, instead of independently measuring and characterizing a battery cell, one of the pre-installed parameter sets was used. The battery chosen for this study is a LGM50 cell, made with NCM811 chemistry, described in O’Kane et al. (2022) and Taylor (2023). The battery model used for this work is a DFN model with simplified active material concentration profile (quartic), as per Subramanian et al. (2005). The O’Kane et al. (2022) parameter set includes degradation parameters which were modified – as per Table 2 – in order to showcase an accelerated degradation simulation for demonstration purposes. All others parameter values are left unaltered.

Lastly, though PyBaMM allows for battery models with built-in thermal models, this part was simulated within Simulink as described in (14). By simulating the thermal model outside of the PyBaMM model, the simulation convergence time is able to be significantly reduced. The same thing was done in Tranter (2021). The thermal parameters are listed in Table 1 based on O’Kane et al. (2022) and the data sheet for the LGM50 cell (Taylor, 2023). Of note, the sides of the cylindrical cell were disregarded when estimating battery surface area (A_{cell}) for (14). This is meant to represent the way in which a real cell would only ever be one of many within a pack and be surrounded by all sides.

Table 1. BYD electric-bus parameters for simulation, adapted from BYD (2022), Taylor (2023), and Prada et al. (2012).

Parameter Name	Value
Mass (M)	20300 kg
Max torque (T_{max})	1100 Nm
Max power (P_{max})	300 kW
Max regenerative power (P_{reg}^{max})	180 kW
Gear ratio (G)	22
Wheel radius (r_w)	0.502 m
Front area (A)	8.20 m ²
Transmission efficiency (η_t)	0.80
Rotational Inertial (k_m)	1.3
Air drag coeff. (C_{drag})	1.3
Rolling resistance coeff. (C_{rr})	1.0
Driver model P and I values	(0.3 and 0.08)
Ambient temperature (T_{amb})	300 K
Mass of battery cell (M_{cell})	0.068 kg
Surface area of battery cell (A_{cell})	0.0007 m ³
Battery cell Heat capacity (C_{pcell})	653.3 J/kg/K
Battery cell convective coeff. (h_{cell})	10 W/m ² /K

Table 2. Battery degradation parameters (Reniers et al., 2019; O’Kane et al., 2022)

Parameter Name	Value
SEI growth model	solvent-diffusion limited
SEI solvent diffusivity	1.25×10^{-20} m ² /s
SEI partial molar volume	5.0×10^{-4} m ³ /mol
Li-plating model	Irreversible
Li-plating kinetic rate const.	5.0×10^{-13} m/s
Initial negative porosity	0.20

4.1 Simulation workflow

Physics based battery models are expressed by dozens of interconnected differential equations. These are implemented and solved within PyBaMM with CasADi, an open-source symbolic math software tool which can be used to represent and solve systems of differential equations (Andersson et al., 2018). CasADi is available in Python, Matlab/Octave and C++. This makes it possible for the battery model to be exported between programs. The workflow required for this project is pictured in Figure 5.

In the first stage of Figure 5, PyBaMM is used to describe the initial battery model. In this stage, the model details, degradation sub-models, parameter set, solution time-step and the simulation inputs (power demand, temperature) and outputs (voltage, capacity lost to SEI and plating, etc.) are all chosen. Then, a short simulation initializes the CasADi model which then makes it possible to extract

the models internal state variables and the integrator and output functions out of the PyBaMM model.

The internal variables (y) is a $[1 \times N]$ array which includes all simulation values at a instant t_0 , where N depends on model options. The integrator is a CasADi function which updates the model internal variables by solving the system of differential equations for a given time-step dt . In the case of this work, the battery time-step is equal to $dt=0.5s$. The integrator function is represented by (15), where i is the array of input parameter values. The output variable function is a set of equations which relates the internal variables (y) and the input values (i) to the output variable values (o), as shown in (16). Each of these three objects can be exported as a file: `y.mat`, `integrator.casadi`, and `outvar.casadi`.

$$y_{n+1} = F_{Int}(y_n, i_n) \quad (15)$$

$$o_n = F_{Out}(y_n, i_n) \quad (16)$$

In the second stage of Figure 5 (now in MATLAB), a Simulink block (`matlab.System` class) loads the internal y variables from the `.mat` file and the integrator and output functions using the CasADi package at start-up. Then, at each simulation step, this simulink block runs the integrator and output functions. A simplified diagram of the simulink is shown in Figure 6. It is composed of the simplified EV model, as described in Section 2; a battery thermal model (implemented outside the battery model itself), based on (14); and the CasADi battery block, which runs the battery model previously declared in PyBaMM. Of note, the CasADi battery block simulates a single representative cell, meaning this model effectively assumes a homogeneous battery pack. As such, the block power input (P_{cell}) is given as a fraction of battery pack power, as calculated in accordance to the EV model in Section 2. Figure 7 shows the power profile required from a battery cell for a given drive cycle period.

With this, a functional PyBaMM model is operational within Simulink. However, the simulation times in Simulink are significantly longer than in PyBaMM. In order to more efficiently run many cycles, the final internal variables y and the cell power and temperature time series are all

exported and saved as files once the MATLAB simulation ends. Then, in the third stage of Figure 5, PyBaMM creates a new model with variables y from the Simulink run as the model initial conditions and uses power and temperature time series as discharge cycle inputs. PyBaMM then runs many charge and discharge cycles, this can be done significantly faster than what's possible in Simulink (Li et al., 2024). After a given number of cycles, the internal variables vector y is saved to file and the Simulink EV model is run once again – this is done to periodically obtain new power and temperature profiles as the battery ages. In this work, there were nine cycles on PyBaMM for every one done in Simulink.

Steps two and three are repeated as many times as is necessary for the simulation experiment. In the case of this work, the goal is to replicate an aging knee point.

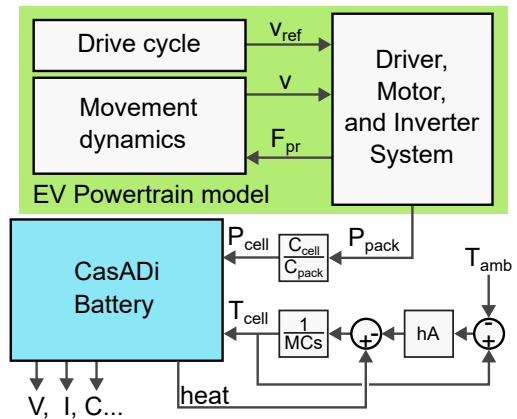


Figure 6. Simplified Simulink model diagram.

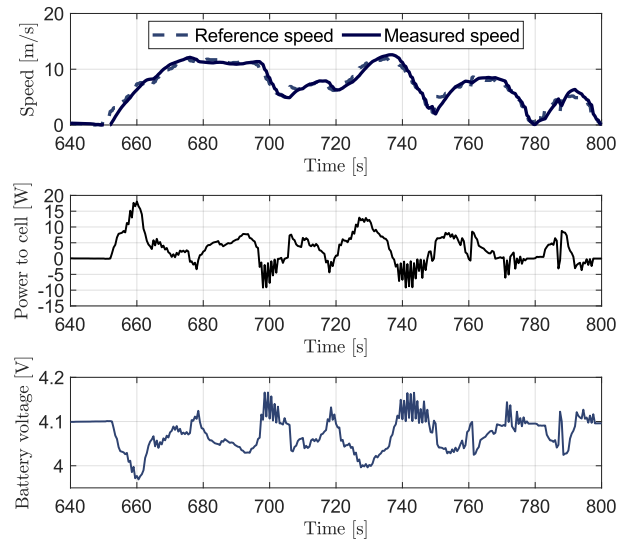


Figure 7. Graphs of vehicle velocity (reference and measured), cell input power, and cell output voltage over a 3 minute period.

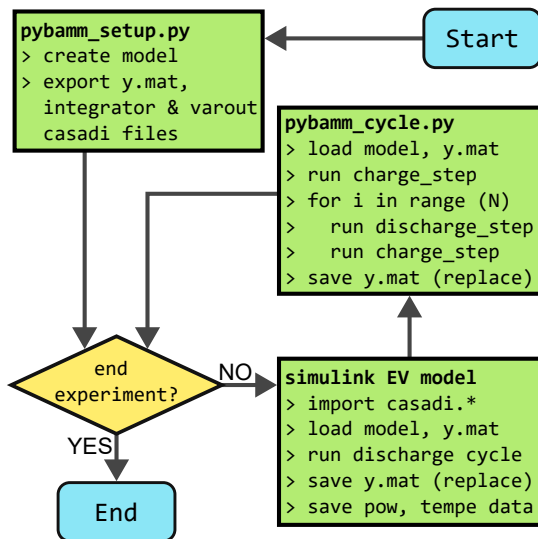


Figure 5. Simulation experiment workflow.

4.2 Results

At the end of each charge and discharge step, porosity and capacity data was saved to file. Figure 8 shows the evolution of capacity loss and negative electrode porosity relative to total battery throughput. Note that capacity

lost to Li-plating has been doubled in value in the plot of Figure 8 so that it is more visible relative to SEI capacity loss.

Initially, the rate of SEI-led capacity loss is elevated as the initial SEI layer is formed; this result is consistent with what has been observed experimentally elsewhere (Yang et al., 2017; Single et al., 2018). Capacity fade then stabilizes and grows linearly with throughput capacity during the “middle” stage of the battery life-cycle, but as “porosity” falls, the rate of Li-plating increases – particularly once porosity is less than 0.05. This is more evident when comparing the cumulative capacity loss due to plating with its linear trend in Figure 8.

After 71 charge and discharge cycles, however, the simulation crashes – the solution fails to converge. This tends to happen as porosity (which is inversely proportional to electrolyte resistivity) approaches zero. This isn’t that bad seeing as, by that point, the battery is quickly approaching its definitive end of life anyway due to the accelerating rate of Li-plating, which increases the risk of short-circuit or thermal runaway. The simulation can be made more stable by adjusting the CasADi solver tolerance settings, but that comes at the cost of solution time. As currently constituted, the simulation takes about 25 hours to solve 71 full cycles (at which point, it crashes). Balancing accuracy, stability and simulation runtime is an important balancing when solving a physics based battery model, this topic is discussed in Li et al. (2024). In the future, this project will aim to better optimize for speed by simplifying the PyBaMM model even further and tinkering with the CasADi solver options.

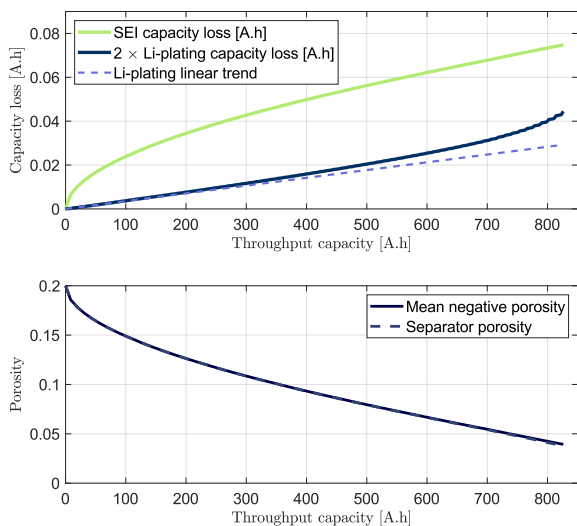


Figure 8. Loss of capacity over SEI growth and Li-plating overtime and Decrease in negative electrode porosity (mean and near separator) overtime.

5. CONCLUSION

The test described in Section 4 of this work is an example of Simulink – a common simulation and testing tool used in many areas of academia – interfacing with PyBaMM – a python library specifically specialized in simulating physics-based electrochemical battery cell models. With

the more complete and complex battery degradation models, it is possible to run more accurate and through battery degradation simulations.

This work has some limitations, however. For one, the simulation itself is merely illustrative due to the artificial degradation variables used for the purposes of demonstrating accelerated degradation. This itself isn’t an issue since the goal of this work is to demonstrate the workflow and viability of Simulink and PyBaMM integration. More important, the simulation is generally slow, taking roughly one day to run 70 cycles. This can be further optimized by simplifying the battery model and tinkering with the CasADi solver options, as described in Li et al. (2024). Additionally, a big reason for the slow simulation time is the small time-steps required to run the EV powertrain models ($dt=0.5$); other applications that don’t require such small time-steps, ie. storage for grid-support, might make for a more appropriate use-case for this kind of simulation.

Future work within this project will focus on using the workflow described here to simulate the Second Life degradation for an electric vehicle battery cell.

REFERENCES

- Alcantara, P.H.F.d. (2022). Estudo da autonomia do e-bus no campus pampulha da UFMG. Tese de Conclusão de Curso, Eng. Elétrica – Universidade Federal de Minas Gerais.
- Andersson, J.A.E., Gillis, J., Horn, G., Rawlings, J.B., and Diehl, M. (2018). CasADi – A software framework for nonlinear optimization and optimal control. *Mathematical Programming Computation*.
- Atalay, S., Sheikh, M., Mariani, A., Merla, Y., Bower, E., and Widanage, W.D. (2020). Theory of battery ageing in a lithium-ion battery: Capacity fade, nonlinear ageing and lifetime prediction. *Journal of Power Sources*, 478, 229026.
- BYD (2022). BYD D9W 20.410 datasheet. Technical report. <https://www.byd.com.br/wp-content/uploads/2022/03/BYD-D9W-20.410-v.-7.0-2022.pdf>.
- Doyle, M., Fuller, T.F., and Newman, J. (1993). Modeling of galvanostatic charge and discharge of the lithium/polymer/insertion cell. *Journal of the Electrochemical society*, 140(6), 1526.
- Edge, J.S., O’Kane, S., Prosser, R., Kirkaldy, N.D., Patel, A.N., Hales, A., Ghosh, A., Ai, W., Chen, J., Yang, J., et al. (2021). Lithium ion battery degradation: what you need to know. *Physical Chemistry Chemical Physics*, 23(14), 8200–8221.
- Ehsani, M., Gao, Y., Longo, S., and Ebrahimi, K. (2018). *Modern electric, hybrid electric, and fuel cell vehicles*. CRC press.
- Fuller, T.F., Doyle, M., and Newman, J. (1994). Simulation and optimization of the dual lithium ion insertion cell. *Journal of the electrochemical society*, 141(1), 1.
- Ganesh, S.V. and D’Arpino, M. (2023). Critical comparison of li-ion aging models for second life battery applications. *Energies*, 16(7), 3023.
- Guo, M., Sikha, G., and White, R.E. (2010). Single-particle model for a lithium-ion cell: Thermal behavior. *Journal of The Electrochemical Society*, 158(2), A122.

- Han, X., Lu, L., Zheng, Y., Feng, X., Li, Z., Li, J., and Ouyang, M. (2019). A review on the key issues of the lithium ion battery degradation among the whole life cycle. *ETransportation*, 1, 100005.
- Hariharan, K.S., Tagade, P., Ramachandran, S., Hariharan, K.S., Tagade, P., and Ramachandran, S. (2018). Theoretical framework of the electrochemical model. *Mathematical Modeling of Lithium Batteries: From Electrochemical Models to State Estimator Algorithms*, 13–32.
- Hu, X., Deng, X., Wang, F., Deng, Z., Lin, X., Teodorescu, R., and Pecht, M.G. (2022). A review of second-life lithium-ion batteries for stationary energy storage applications. *Proceedings of the IEEE*, 110(6), 735–753.
- Hu, X., Feng, F., Liu, K., Zhang, L., Xie, J., and Liu, B. (2019). State estimation for advanced battery management: Key challenges and future trends. *Renewable and Sustainable Energy Reviews*, 114, 109334.
- Hu, X., Li, S., and Peng, H. (2012). A comparative study of equivalent circuit models for li-ion batteries. *Journal of Power Sources*, 198, 359–367.
- Hu, X., Xu, L., Lin, X., and Pecht, M. (2020). Battery lifetime prognostics. *Joule*, 4(2), 310–346.
- Lee, S.B. and Onori, S. (2021). A robust and sleek electrochemical battery model implementation: a matlab® framework. *Journal of The Electrochemical Society*, 168(9), 090527.
- Li, R., O’Kane, S., Huang, J., Marinescu, M., and Offer, G.J. (2024). A million cycles in a day: Enabling high-throughput computing of lithium-ion battery degradation with physics-based models. *Journal of Power Sources*, 598, 234184.
- Mahmoudi, A., Soong, W.L., Pellegrino, G., and Armando, E. (2015). Efficiency maps of electrical machines. *2015 IEEE Energy Conversion Congress and Exposition (ECCE)*, 2791–2799. URL <https://api.semanticscholar.org/CorpusID:99322>.
- Marquis, S.G. (2020). *Long-term degradation of lithium-ion batteries*. Ph.D. thesis, University of Oxford.
- Martinez-Laserna, E., Gandiaga, I., Sarasketa-Zabala, E., Bada, J., Stroe, D.I., Swierczynski, M., and Goikoetxea, A. (2018). Battery second life: Hype, hope or reality? a critical review of the state of the art. *Renewable and Sustainable Energy Reviews*, 93, 701–718.
- Miri, I., Fotouhi, A., and Ewin, N. (2021). Electric vehicle energy consumption modelling and estimation—a case study. *International Journal of Energy Research*, 45(1), 501–520.
- Müller, D., Dufaux, T., and Birke, K.P. (2019). Model-based investigation of porosity profiles in graphite anodes regarding sudden-death and second-life of lithium ion cells. *Batteries*, 5(2), 49.
- Newman, J. and Balsara, N.P. (2021). *Electrochemical systems*. John Wiley & Sons.
- O’Kane, S.E., Ai, W., Madabattula, G., Alonso-Alvarez, D., Timms, R., Sulzer, V., Edge, J.S., Wu, B., Offer, G.J., and Marinescu, M. (2022). Lithium-ion battery degradation: how to model it. *Physical Chemistry Chemical Physics*, 24(13), 7909–7922.
- Oliveira, V.M.R.d., Remédios, V.F.d., Donadel, C.B., Santos, W.M.d., Có, M.A., Melo, V.S.d., and Nunes, R.B. (2023). Electric vehicles modeling: A review. In *2023 15th IEEE International Conference on Industry Applications (INDUSCON)*, 285–292. IEEE.
- Prada, E., Di Domenico, D., Creff, Y., Bernard, J., Sauvant-Moynot, V., and Huet, F. (2012). Simplified electrochemical and thermal model of lifepo4-graphite li-ion batteries for fast charge applications. *Journal of The Electrochemical Society*, 159(9), A1508.
- Reniers, J.M., Mulder, G., and Howey, D.A. (2019). Review and performance comparison of mechanical-chemical degradation models for lithium-ion batteries. *Journal of The Electrochemical Society*, 166(14), A3189–A3200.
- Richardson, G.W., Foster, J.M., Ranom, R., Please, C.P., and Ramos, A.M. (2022). Charge transport modelling of lithium-ion batteries. *European Journal of Applied Mathematics*, 33(6), 983–1031.
- Single, F., Latz, A., and Horstmann, B. (2018). Identifying the mechanism of continued growth of the solid-electrolyte interphase. *ChemSusChem*, 11(12), 1950–1955.
- Subramanian, V.R., Diwakar, V.D., and Tapriyal, D. (2005). Efficient macro-micro scale coupled modeling of batteries. *Journal of The Electrochemical Society*, 152(10), A2002.
- Sulzer, V., Marquis, S.G., Timms, R., Robinson, M., and Chapman, S.J. (2021). Python battery mathematical modelling (PyBaMM). *Journal of Open Research Software*, 9(1).
- Taylor, N. (2023). LG INR 21700 M50 battery datasheet. <https://www.batterydesign.net/lg-21700-m50/>.
- Thomas, K.E., Newman, J., and Darling, R.M. (2002). Mathematical modeling of lithium batteries. In *Advances in Lithium-ion Batteries*, chapter 12. Kluwer Academic Publisher.
- Tranter, T.G. (2021). PyBaMM Simulink integration example. https://github.com/FaradayInstitution/pybamm_simulink_example.
- Waldmann, T., Wilka, M., Kasper, M., Fleischhammer, M., and Wohlfahrt-Mehrens, M. (2014). Temperature dependent ageing mechanisms in lithium-ion batteries—a post-mortem study. *Journal of power sources*, 262, 129–135.
- Yang, X.G., Leng, Y., Zhang, G., Ge, S., and Wang, C.Y. (2017). Modeling of lithium plating induced aging of lithium-ion batteries: Transition from linear to nonlinear aging. *Journal of Power Sources*, 360, 28–40.
- Zhou, Y.L. (2007). Modeling and simulation of hybrid electric vehicles.